Performance improvement of InGaN/GaN multiple quantum well visible-light photodiodes by optimizing TEGa flow*

Bin Li(黎斌)[2,3], Shan-Jin Huang(黄善津)[2], Hai-Long Wang(王海龙)[2], Hua-Long Wu(吴华龙)[2], Zhi-Sheng Wu(吴志盛)[1], Gang Wang(王钢)[1], and Hao Jiang(江灏)[1,†]

[1] *State Key Laboratory of Optoelectronic Materials and Technologies, School of Electronics and Information Technology, Sun Yat-Sen University, Guangzhou* 510275, *China*

[2] *School of Physics and Engineering, Sun Yat-Sen University, Guangzhou* 510275, *China*

[3] *The Open University of Guangdong & Guangdong Polytechnic Institute, Guangzhou* 510091, *China*

(Received 19 January 2017; revised manuscript received 17 April 2017; published online 20 June 2017)

The performance of an InGaN/GaN multiple quantum well (MQW) based visible-light Schottky photodiode (PD) is improved by optimizing the source flow of TEGa during InGaN QW growth. The samples with five-pair InGaN/GaN MQWs are grown on sapphire substrates by metal organic chemical vapor deposition. From the fabricated Schottky-barrier PDs, it is found that the smaller the TEGa flow, the lower the reverse-bias leakage is. The photocurrent can also be enhanced by depositing the InGaN QWs with using lower TEGa flow. A high responsivity of 1.94 A/W is obtained at 470 nm and −3-V bias in the PD grown with optimized TEGa flow. Analysis results show that the lower TEGa flow used for depositing InGaN may lead to superior crystalline quality with improved InGaN/GaN interface, and less structural defects related non-radiative recombination centers formed in the MQWs.

Keywords: visible-light photodiodes, quantum wells, triethylgallium, oxidized iridium

PACS: 73.50.Pz, 73.61.Ey, 78.66.Fd **DOI:** 10.1088/1674-1056/26/8/087307

1. Introduction

Nowadays, applications such as visible light communication, biophotonics, and fluorescence spectroscopy highly require the efficient photodetectors working in the visible-light wavelength region.[1] The InGaN ternary alloys are promising semiconductors for visible-light detection because of their direct and tunable band gap energy from 0.7 eV to 3.4 eV, covering the entire visible region by varying the indium (In) composition. Up to now, the InGaN-based photodetectors, however, still suffer from the large leakage current and poor spectral response characteristics, due to the presence of a high density point and line defects, and phase separation and composition-pulling effects in InGaN epitaxial layers.[2,3] These problems generally become more serious as the In content and layer thickness increase.

The InGaN/GaN multi-quantum well (MQW)-based photodetector has been used as an alternative to overcome the technological problems.[4,5] The reported InGaN/GaN MQWs-based photodiodes demonstrated the superior characteristics of low dark current, high detection contrast, and high responsivity resulting from the internal gain mechanism by the polarization field.[6] Further performance improvement in terms of quantum efficiency has been shown possibly by designing the device with appropriate parameters such as the number of QWs, the thickness values and doping levels of barrier and blocking layers.[7] Besides the structure design, the effects of growth parameters are also important for improving the performance. For the InGaN/GaN MQWs grown with the common metal organic chemical vapor deposition (MOCVD) method, the structural and optical properties are very sensitive to the main growth parameters such as growth temperature, pressure, and gas flows. The influences of trimethylindium (TMIn),[8] ammonia,[9] and hydrogen[10] on the optical and electrical characteristics of InGaN/GaN-MQWs-based optoelectronics have been widely investigated. However, the effect of the triethylgallium (TEGa) flow, which is usually used as the Ga source when growing InGaN QWs, is seldom reported.

In this work, the effects of the TEGa flow on the optical and structural properties of $In_xGa_{1-x}N(x \sim 0.2)$/GaN MQWs are first investigated. Then the planar Schottky photodiodes are fabricated on the MQW wafer samples. Reduced leakage and enhanced photocurrent are obtained in the devices with superior MQW properties. The mechanisms for the improvements are also analyzed.

2. Experimental procedure

The InGaN/GaN MQW samples were grown on (0001) sapphire substrates by using a low-pressure MOCVD system. TMIn and NH_3 were used as precursors for In and N, respectively. TEGa was used as the Ga source for depositing InGaN QWs while trimethylgallium (TMGa) was used for growing GaN layers. During the growth of InGaN/GaN MQWs, the

*Project supported by the Science and Technology Major Project of Guangdong Province, China (Grant Nos. 2014B010119003 and 2015B010112001).

†Corresponding author. E-mail: stsjiang@mail.sysu.edu.cn

© 2017 Chinese Physical Society and IOP Publishing Ltd

carrier gas was switched from H_2 to N_2 to avoid compromising the In incorporation. The sample epistructure consists of a 25-nm-thick nucleation layer grown at 530 °C, a 4-μm-thick undoped GaN layer deposited at 1050 °C, a five-periods $In_xGa_{1-x}N(x \sim 0.2)$/GaN MQWs and a 35-nm-thick GaN cap layer. The QWs and quantum barriers (QBs) were grown at 715 °C and 815 °C, respectively. Before the temperature was ramped up to grow QB, a 1-nm-thick GaN protecting layer was deposited right after the growth of InGaN QW. Table 1 lists the growth conditions of our three samples.

The Schottky-barrier photodiodes (SBPD) were fabricated by the following procedure: Ohmic contact of Ti (15 nm)/Al(80 nm)/Ni(20 nm)/Au(60 nm) was deposited via electron-beam evaporation followed by annealing in a rapid thermal annealing (RTA) system at 780 °C for 30 s in N_2 ambient. A 10-nm-thick semitransparent iridium (Ir) film was electro-beam deposited as the Schottky contacts each with a diameter of 150 μm. After that, the Schottky contacts were annealed by RTA at 500 °C for 1 min in O_2 ambient for forming IrO_2 Schottky contacts.[11] Prior to device fabrication, the epitaxial samples were treated in $HCl + H_2O_2$ for 10 min to remove the surface oxides and other impurities.

Structural properties of the MQW samples were investigated by an ω–2θ method of high resolution x-ray diffraction (HR-XRD). Simulations with using LEPTOS software were carried out to estimate the values of In content and thickness of the QWs and QBs. Optical properties were characterized by the temperature-dependent photoluminescence (TDPL) measurements in a range of 8 K–300 K by using a 325-nm-wavelength 25-mW He–Cd laser as an excitation source. Current–voltage (I–V) characteristics of the photodiodes were measured by using a Keithley 4200-SCS characterization system at room temperature under dark and illumination conditions respectively. The spectral photoresponses were measured by using a light source of a xenon lamp, a monochromator with 1200 g/mm grating, and a calibrated Si photodiode.

3. Results and discussion

Figure 1 shows the ω–2θ scans for (0004) reflection of the three samples grown with different TEGa flows. The strongest peak at $\theta \sim 36.5°$ comes from the (0004) plane underneath the undoped-GaN and satellite peaks originate from the InGaN/GaN MQWs. By fitting the position and the relative intensity of the light-order satellite peaks,[12] the values of QW/QB thickness and the In content in MQWs are estimated. The obtained results are also summarized in Table 1. In the calculation, the full strain condition is assumed to hold for the InGaN QWs, which is usually valid for such thin QWs. It can be seen that the In content increases with TEGa flow increasing, which may be attributed to the enhanced In incorporation by the higher growth rate under the larger TEGa flow.[13]

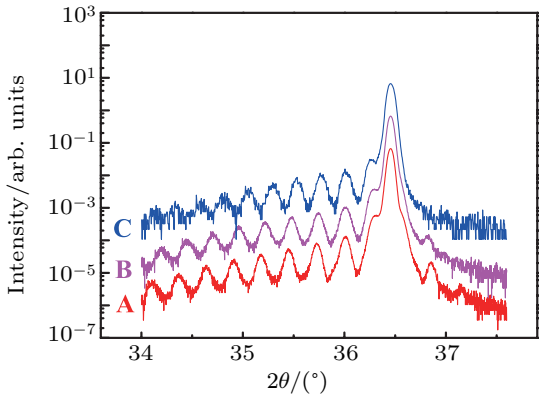


Fig. 1. (color online) HR-XRD $\omega/2\theta$ scans for the (0004) plane of the samples grown with different TEGa flows.

For sample A, a well-defined satellite peak up to the 8th order can be clearly distinguished indicating the high quality of the prepared MQWs which is better than that of the usual $In_xGa_{1-x}N(x \sim 0.2)$/GaN MQWs with the observed satellite peak up to 2nd–4th.[14,15] Comparing with sample A, a deterioration of the satellite peaks is clearly presented in sample C, meaning that the interface between QW and QB is rougher in sample C.

It is well known that the full width at half maximum (FWHM) of the satellite peak will be broadened by the interface roughness of an MQW structure. The interface roughness can therefore be evaluated according to the FWHM change of satellite peak with increasing order of the peak.[16] Using the method described in Ref. [16], the interface roughness values are calculated to be 0.3%, 1.4%, and 2.4% for samples A–C, respectively. It can be easily found that the roughness increases with TEGa flow increasing.

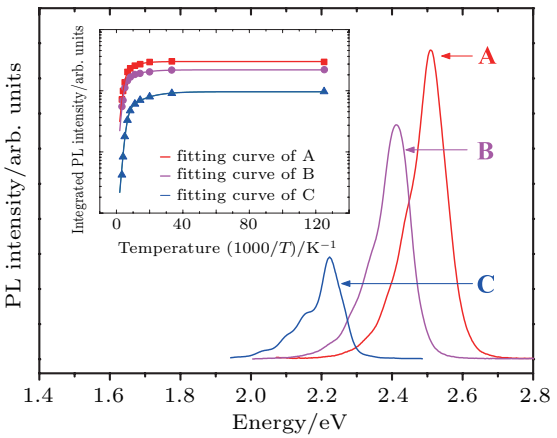


Fig. 2. (color online) PL spectra of InGaN/GaN MQWs grown with different TEGa flows measured at 8 K. Inset shows the Arrhenius plots of the integrated TDPL intensity of samples A, B, and C. The solid lines are the corresponding fitting curves.

Figure 2 shows the PL spectra of the three InGaN/GaN MQWs samples measured at 8 K. For sample A we observe a strong single emission peak at 2.51 eV. With TEGa

flow increasing from 4.47 μmol/min to 5.44 μmol/min, the emission peak shifts to the lower energy of 2.23 eV, which can be attributed to the more In adatoms incorporating into the QWs and quantum-confined Stark effect (QCSE) induced by the piezoelectric field in MQWs increasing with the QW thickness.[17] It can also be seen that the peak intensity decreases with TEGa flow increasing. Moreover, a shoulder peak at 2.18 eV is observed in sample C. It is known that In-rich clusters caused by inhomogeneous distribution of In adatoms in the InGaN QW layer would lead to the appearance of the lower energy peak.[18,19] Therefore, the single and strong PL peak of sample A can be ascribed to the more homogeneous distribution of In adatoms in the QW layer by the low TEGa flow. A possible explanation for this effect is that during the QW growth the In adatoms undergo a dynamic equilibrium between absorption and desorption. Reducing the TEGa flow (growth rate) may enhance desorption of solitary In adatoms, leading to an improved distribution of In adatoms in InGaN QWs.

Thermal-quenching analysis by the TDPL measurements is an effective way to evaluate the crystalline qualities of InGaN/GaN MQWs.[20,21] It is generally known that a number of nonradiative recombination centers (NRCs) are formed in InGaN QWs and the activation energy of these NRCs is always smaller than the total QW binding energy of electrons and holes. Accordingly, the luminescence thermal quenching of the InGaN/GaN MQWs is actually dominated by the nonradiative recombination process.[22] The integrated PL intensity can therefore be expressed as a function of NRC density in MQWs and the activation energy of NRC in the thermal activated process. The following expression considering two nonradiative recombination centers is usually used for evaluating the NRC density and the activation energy:[23]

$$I(T)/I(0)=1\Big/\left[1+\sum \alpha_i \exp\left(-\frac{E_{\alpha i}}{k_{\mathrm{B}}T}\right)\right],$$

where α_i are rate constants related to the density of NRCs, $E_{\alpha i}$ are the activation energies of the corresponding NRCs, and k_{B} is the Boltzmann constant. We record the PL spectra in a temperature range of 8 K–300 K. Using the equation, the integrated PL intensities are well fitted as shown in the inset of Fig. 2, and part of the fitting parameters are also summarized in Table 1.

Table 1. Growth conditions, characterization results, and the fitting parameters of the normalized temperature-dependent PL integrated intensities for samples A, B, and C.

Sample	TEGa	Structural parameters			Interface	Fitting parameters			
	flow/(μmol/min)	QW/nm	QB/nm	In content	roughness	α_1	E_1/meV	α_2	E_2/meV
A	4.47	2.62	17.05	19.2%	0.3%	1.04	14.7	40.01	70.21
B	5.05	2.80	17.85	20.2%	1.4%	0.77	10.7	46.10	74.05
C	5.44	2.89	19.46	22.8%	2.4%	1.75	9.04	203.3	69.66

As can be seen from Table 1, the rate constants α_1 and α_2 of samples A and B are much smaller than those of sample C, which means that the density of effective NRCs is reduced by lowering the TEGa flow. The relatively small rate constants of α_1 and α_2 obtained in sample A indicate the superior crystalline quality of InGaN/GaN MQWs. These are well consistent with the HR-XRD and PL results. On the other hand, for the dominant α_2-type NRCs, the values of activation energy E_2 ($\sim$ 70 meV) of the three samples change little, suggesting that they might have the same origin of NRCs because of their similar activation energies. Dislocations are the likely candidate responsible for these NRCs, due to the similar characters and densites in all of the three samples. However, this possibility is contradicted by the results obtained by using quite different NRC densities between sample C and sample A or B. It has been reported that the large-size In clusters split into small clusters (i.e., more homogeneously distributed In adatoms) may enhance the screen effect of NRCs.[22] Therefore, we speculate that the lower density of effective NRCs in sample A is ascribed to the suppression of In segregation.

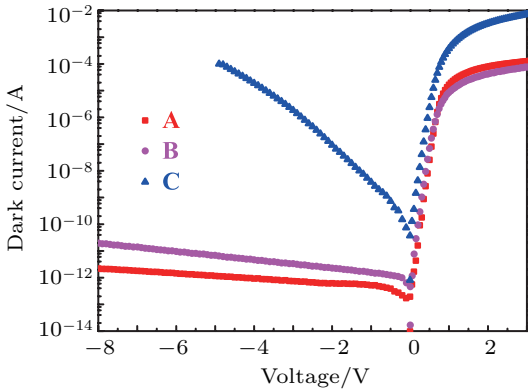


Fig. 3. (color online) Dark *I*–*V* curves for photodiodes fabricated on samples A–C. The diameter of the Schottky contact is 150 μm.

The dark *I*–*V* characteristics of the three SBPD samples are shown in Fig. 3. At a reverse bias voltage of 2 V, the dark currents of the samples A–C are about 6.2×10^{-13} A, 2.3×10^{-12} A, and 9.2×10^{-8} A, respectively. With increasing the reverse bias voltage, the dark currents of samples A and B increase gradually, whereas that of sample C increases dramatically. The forward/reverse current ratio at

+/ − 2 V of samples A–C are about 1.28×10^8, 1.86×10^7, and 3.59×10^4 respectively, indicating that the sample grown with lower TEGa flow has a superior rectifying characteristic. This improvement is ascribed to the suppressed structural defects in the InGaN/GaN MQWs by the low TEGa flow. It has been proposed that the dislocations/V-defects or In clusters be correlated to the localized leakage paths in the InGaN/GaN MQW system.[24] Since the dislocations in the GaN grown on sapphire substrates are mainly from underneath the GaN buffer, the extra dislocations generated during the growth of InGaN/GaN MQWs might be marginal and can be safely ignored compared with the dislocations penetrated from underneath the GaN layers. This assumption is supported by the fact that all the samples are grown under identical growth conditions for the GaN buffer layer, and by the (105) reciprocal space mapping results (not shown here) which reveal that all the InGaN/GaN MQWs are coherently strained on the GaN buffer. Therefore, the suppressed In clusters by the low TEGa flow, rather than the dislocation reduction, are considered to be the reason for the leakage improvement in our case.

Table 2. SBH and n values of SBPD samples A–C obtained from the TE and TFE models.

Sample	TE model		TFE model	
	Φ_b/eV	n	Φ_b/eV	n
A	1.13	1.70	1.54	1.22
B	1.10	1.65	1.50	1.40
C	1.00	1.75	1.39	1.55

To evaluate the Schottky-contact parameters, we analyze the forward I–V curves of SBPD samples A–C by using the thermionic emission (TE) model.[25] The Schottky barrier height (SBH) and ideality factor (n) of sample A are determined to be 1.13 eV and 1.70, respectively, by using the theoretical Richardson constant of $A^* = \alpha m^* q k^2/2\pi\hbar = 26$ A·cm^{-2}·K^{-2}. For sample C, the SBH and n are 1.00 eV and 1.75, respectively. These data indicate that the increasing of the TEGa flow causes the SBH to decrease and the ideality factor to increase. Moreover, the obtained ideality factors larger than 1.5 suggest that the TE model is not adequate for explaining the transport characteristics of our SBPD samples.[25] For this reason, the I–V curves are also analyzed by using the thermionic field emission (TFE) model. The obtained values of SBH and n of sample A are 1.54 eV and 1.22, respectively, while those of sample C are 1.39 eV and 1.55. The values of n extracted from the TFE model show a similar changing trend to those obtained by the TE model, but closer to 1 (see Table 2), meaning that the thermally-assisted-tunneling mechanism is more suitable for the forward current transport in samples A–C.

On the other hand, the leakage current transport mechanisms in the SBPD samples are also investigated. Dark reverse I–V curves are measured at different temperatures ranging from 293 K to 353 K. We find that the current transport fits well the Frenkel–Poole emission model which is expressed as[26]

$$J = CE\exp\left[-\frac{q\left(\Phi_t - \sqrt{qE/\pi\varepsilon_0\varepsilon_s}\right)}{kT}\right]. \tag{1}$$

From Eq. (1), $\log(J/E)$ should be a linear function of $E^{0.5}$, i.e,

$$\begin{aligned}\log(J/E) &= \frac{q}{kT}\sqrt{\frac{qE}{\pi\varepsilon_0\varepsilon_s}} - \frac{q\Phi_t}{kT} + \log C \\ &= R(T)\sqrt{E} + S(T),\end{aligned} \tag{2}$$

$$R(T) = \frac{q}{kT}\sqrt{\frac{q}{\pi\varepsilon_0\varepsilon_s}}, \tag{2a}$$

$$S(T) = -\frac{q\Phi_t}{kT} + \log C, \tag{2b}$$

where E is the electric field in the semiconductor barrier, Φ_t is the barrier height for electron emission from the trapped state, ε_s is the relative dielectric permittivity at high frequency, T is the temperature, ε_0 is the permittivity of free space, and k is Boltzmann's constant. The $R(T)$ and $S(T)$ values at different temperatures can be obtained by calculating the slopes and intercepts of $\log(J/E)$ and $E^{0.5}$ curves at different temperatures.

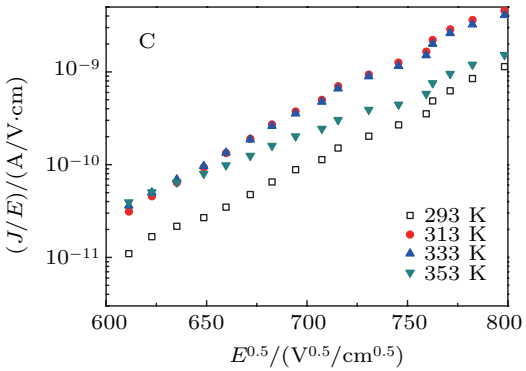


Fig. 4. (color online) Plots of $\log(J/E)$ versus $E^{0.5}$ for sample C SBPD.

Figure 4 shows the plots of reverse J/E as a function of $E^{0.5}$ for sample C SBPD measured at different temperatures. A linear dependence of $\log(J/E)$ on E can be observed. J is also observed to increase with temperature increasing. According to Eqs. (2a) and (2b), $\varepsilon_s = 5.42$ and $\Phi_t = 0.142$ eV can be obtained. The value ε_s for sample C is in agreement with the reported values (5.35 for GaN and 5.8 for InN).[27] The extracted value $\Phi_t = 0.142$ eV suggests that the leakage current in sample C SBPDs is due to the trap-assisted current from the trap states located ~ 0.142 eV below the conduction band edge of GaN.

For sample A SBPD, we find that the Frenkel–Poole process with linear $\ln(J/E)$ versus $E^{0.5}$ relation cannot explain the leakage current properties any more. Figure 5 illustrates the temperature-dependent reverse dark $\log J$ versus $\log E$ curves measured on sample A SBPD. It can be seen that the leakage

current density increases slowly with electric field increasing. Under the same bias voltage, the leakage $\log J$ increases almost linearly with the increase of temperature. At a temperature of 293 K, the linear slope of the $\log J$ versus $\log E$ is about 1.11, indicating that the surface leakage current is the dominant leakage mechanism.[27] Comparing with the sample C SBPD, the decreased leakage current in the sample A device might be attributed to the reduced localized leakage paths associated with the In segregation.

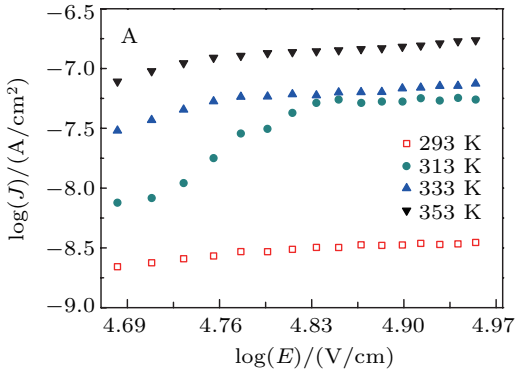


Fig. 5. (color online) Measured reverse dark $\log J$ versus $\log E$ curves for sample A SBPD.

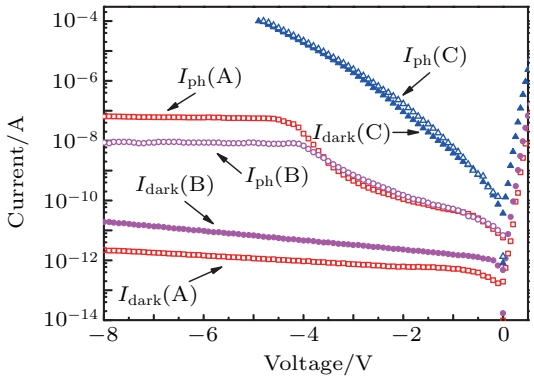


Fig. 6. (color online) *I*–*V* curves of sample A–C PD under dark and illuminated conditions.

Figure 6 shows the *I*–*V* characteristics of samples A–C under the illuminated and dark conditions. A blue light-emitting diode (LED) with a peak wavelength of 450 nm is used as a light source. Due to the large leakage current, the measured photocurrent of sample C is difficult to distinguish from the dark current. For samples A and B, it can be seen that the photocurrent increases exponentially with increasing the reverse bias voltage and is saturated after the reverse bias has become greater than 4 V. The increase of photocurrent is mainly ascribed to the enlargement of the depletion region with increasing the reverse bias, while the saturation at about −4 V is attributed to the full depletion of the MQW region.[5] Compared with sample B, sample A has a large photocurrent, which is considered to be as a result of less recombination centers of photo-generated carriers formed in the MQW region.

Figure 7 shows the spectral responses of sample A. The photoresponse between 360 nm and 470 nm is due to the light absorption in InGaN QWs. The spectral responsivity decreases in the short wavelength region, owing to the light absorption of oxidized Ir Schottky contact as shown in the inset of Fig. 7. A zero-bias peak responsivity of 35.5 mA/W is obtained at 470 nm (2.64 eV), corresponding to an external quantum efficiency (EQE) of 9.4%. The difference between the absorption edge and the PL peak is ascribed to the weakened QCSE effect by the Schottky barrier.[28] As the reverse bias increases, the peak responsivity increases and reaches 1.94 A/W (EQE of 511.8%) at 470 nm and −3 V. This result suggests the existence of high internal gain in the SBPD of sample A.[29] One possible origin of this internal gain is an increased electron injection at the Schottky contact due to the barrier-height lowering when photo-generated holes are trapped at the surface sites.[30] Further improvement is believed to be achieved by optimizing the MQW structure such as the number of QWs and the barrier layer thickness.

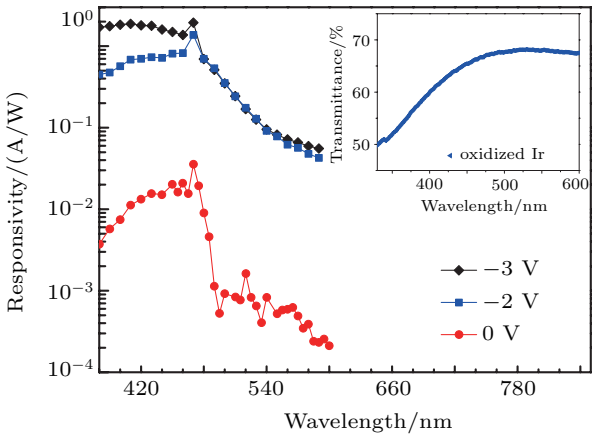


Fig. 7. (color online) Spectral responses of sample A PD at different reverse bias voltages. The inset shows the optical transmittance of oxidized Ir Schottky contact.

4. Conclusions

In this work, the performances of $In_xGa_{1-x}N(x \sim 0.2)$/GaN MQWs-based visible-light Schottky photodiodes are shown to be improved by optimizing the TEGa flow during the MOCVD growth of InGaN QWs. The *I*–*V* characteristics show that the device with InGaN QWs deposited by lower TEGa flow has lower leakage current and higher photocurrent. Peak responsivities of 355 mA/W and 1.94 A/W are obtained at 470 nm under 0 V and −3 V, respectively. Analysis results on structural and optical properties of InGaN/MQWs indicate that superior crystalline quality of InGaN/GaN MQWs in terms of better QW/QB interface, more homogeneous distribution of In adatoms, and less recombination-center defects can be achieved by adopting low TEGa flow, which may account for the improved performances of the photodiodes.

References

[1] Muñoz E, Monroy E, Pau J L, Calle F, Omnès F and Gibart P 2001 *J. Phys.: Condens. Matter* **13** 7115

[2] Pantha B N, Wang H, Khan N, Lin J Y and Jiang H X 2011 *Phys. Rev. B* **84** 075327

[3] Li S X, Yu K M, Wu J, Jones R E, Walukiewicz W, Ager J W, Shan W, Haller E E, Lu H and Schaff W J 2006 *Physica B* **376–377** 432

[4] Chiou Y Z, Su Y K, Chang S J, Gong J, Lin Y C, Liu S H and Chang C S 2003 *IEEE J. Quantum Electron.* **39** 681

[5] Rivera C, Pau J L, Naranjo F B and Muñoz E 2004 *Phys. Status Solidi A* **201** 2658

[6] Rivera C, Pau J L and Muñoz E 2006 *Appl. Phys. Lett.* **89** 263505

[7] Pereiro J, Rivera C, Navarro A and Munoz E 2009 *IEEE J. Quantum Electron.* **45** 617

[8] Kim T K, Shim S K, Yang S S, Son J K and Hong Y K 2007 *Curr. Appl. Phys.* **7** 469

[9] Oliver R A, Kappers M J, Humphreys C J and Briggs G A D 2004 *J. Cryst. Growth* **272** 393

[10] Piner E L, Behbehani M K, Elmasry N A, Mcintosh F G and Roberts J C 1997 *Appl. Phys. Lett.* **70** 461

[11] Li B, Zhang L X, Wu Z S, Wang G and Jiang H 2015 *IEEE Photon. Technol. Lett.* **27** 2300

[12] Smeeton T M, Kappers M J, Barnard J S, Vickers M E and Humphreys C J 2003 *Appl. Phys. Lett.* **83** 5419

[13] Keller S, Keller B P, Kapolnek D, Abare A C and Masui H 1996 *Appl. Phys. Lett.* **68** 3147

[14] Song S W, Liu Y, Liang H W, Xia X C and Zhang K X 2013 *Chin. J. Lumin.* **34** 744

[15] Bayram C and Razeghi M 2009 *J. Vac. Sci. Technol. B* **27** 1784

[16] Pan Z, Wang Y T, Zhuang Y, Lin Y W and Zhou Z Q 1999 *Appl. Phys. Lett.* **75** 223

[17] Chichibu S F, Abare A C, Mack M P, Minsky M S and Deguchi T 1999 *Mater. Sci. Eng. B* **59** 298

[18] Lin Y S, Ma K J, Hsu C, Feng S W and Cheng Y C 2000 *Appl. Phys. Lett.* **77** 2988

[19] Lai Y L, Liu C P and Chen Z Q 2005 *Appl. Phys. Lett.* **86** 121915

[20] Watanabe S, Yamada N, Nagashima M, Ueki Y and Sasaki C 2003 *Appl. Phys. Lett.* **83** 4906

[21] Dai Q, Schubert M F, Kim M H and Kim J K 2009 *Conference on Lasers & Electro-optics* **94** 111109

[22] Wang Y, Pei X J, Xing Z G, Guo L W and Jia H Q 2007 *J. Appl. Phys.* **101** 033509

[23] Bimberg D, Sondergeld M and Grobe E 1971 *Phys. Rev. B* **4** 3451

[24] Meneghini M, Tazzoli A, Butendeich R, Hahn B, Meneghesso G and Zanoni E 2010 *IEEE Electron Dev. Lett.* **31** 579

[25] Chen D J, Huang Y, Liu B, Xie Z L, Zhang R, Zheng Y D, Wei Y and Narayanamurti V 2009 *J. Appl. Phys.* **105** 063714

[26] Arslan E, Bütün S and Ozbay E 2009 *Appl. Phys. Lett.* **94** 142106

[27] Han D P, Oh C H, Kim H, Shim J I, Kim K S and Shin D S 2015 *IEEE Trans. Electron Dev.* **62** 587

[28] Rivera C, Pau J L, Pereiro J and Muñoz E 2004 *Superlattices and Microstructures* **36** 849

[29] Jiang H, Nakata N, Zhao G Y, Ishikawa H, Shao C L, Egawa T, Jimbo T and Umeno M 2001 *Jpn. J. Appl. Phys.* **40** L505

[30] Klingenstein M, Kuhl J, Rosenzweig J, Moglestue C, Hulsmann A, Schneider J and Kohler K 1994 *Solid State Electron.* **37** 333